

Direct measurements of the kinematics and dynamics of bat flight

Xiaodong Tian, Jose Iriarte-Diaz, Kevin Middleton, Ricardo Galvao, Emily Israeli, Abigail Roemer, Allyce Sullivan, Arnold Song, Sharon Swartz and Kenneth Breuer

Brown University, Providence, RI 02912, USA

E-mail: kbreuer@brown.edu

Received 25 July 2006

Accepted for publication 20 November 2006

Published 22 December 2006

Online at stacks.iop.org/BB/1/S10

Abstract

Experimental measurements and analysis of the flight of bats are presented, including kinematic analysis of high-speed stereo videography of straight and turning flight, and measurements of the wake velocity field behind the bat. The kinematic data reveal that, at relatively slow flight speeds, wing motion is quite complex, including a sharp retraction of the wing during the upstroke and a broad sweep of the partially extended wing during the downstroke. The data also indicate that the flight speed and elevation are not constant, but oscillate in synchrony with both the horizontal and vertical movements of the wing. PIV measurements in the transverse (*Treffitz*) plane of the wake indicate a complex ‘wake vortex’ structure dominated by a strong wing tip vortex shed from the wing tip during the downstroke and either the wing tip or a more proximal joint during the upstroke. Data synthesis of several discrete realizations suggests a ‘cartoon’ of the wake structure during the entire wing beat cycle. Considerable work remains to be done to confirm and amplify these results.

1. Introduction

Although the tools for the analysis and design of vehicles optimized for steady flight are well developed, the mechanics of highly unsteady flight remains uncertain. This is an issue of growing interest, driven by the desire to build vehicles that can perform extreme unsteady aerodynamic maneuvers. As engineering materials, actuators and controls have become more sophisticated, we are able to think about mimicking the natural world. Such efforts, however, have been hampered by the lack of development of actuators for biomimetic flight, and at a more fundamental level, by deep gaps in our understanding of the basic mechanics of the highly unsteady, three-dimensional and complex character of animal flight. Flapping flight is the single most evolutionarily successful mode of animal locomotion: there are today over 1200 species of bats, more than 10 000 living species of flying birds, and somewhere between millions and tens of millions of species of flying insects. Understanding how animals fly is not only central to providing insight into the biological world; the rich

diversity of mechanisms of animal flight can provide abundant inspiration for engineered design.

It is therefore surprising that we understand so much less about animal flight than we do about terrestrial locomotion (Cavagna *et al* 1977, Farley and McMahon 1992, Blickhan and Full 1993, Farley and Ferris 1998, Dickinson *et al* 2000, Alexander 2003, Biewener 2003). With few exceptions, it is only in the last 20 years that biologists have begun to rigorously address this knowledge gap. Recently, however, application of fluid dynamic approaches has revolutionized understanding of insect flight. Computational fluid dynamics, detailed force measurements from tethered animals and physical modeling of wake structure, using both smoke visualization and particle image velocimetry (PIV), have been integrated to reveal mechanisms responsible for the generation of aerodynamic forces in insects to a degree previously almost unimaginable (Edwards and Cheng 1982, Ellington 1984, Heinzel and Gewecke 1987, Grodnitsky and Dudley 1996, VandenBerg and Ellington 1997a, 1997b, Willmott and Ellington 1997a, 1997b, Liu *et al* 1998, Dickinson *et al* 2000, Müller *et al* 2000, Birch and Dickinson 2001, Dickinson 2001, Sane

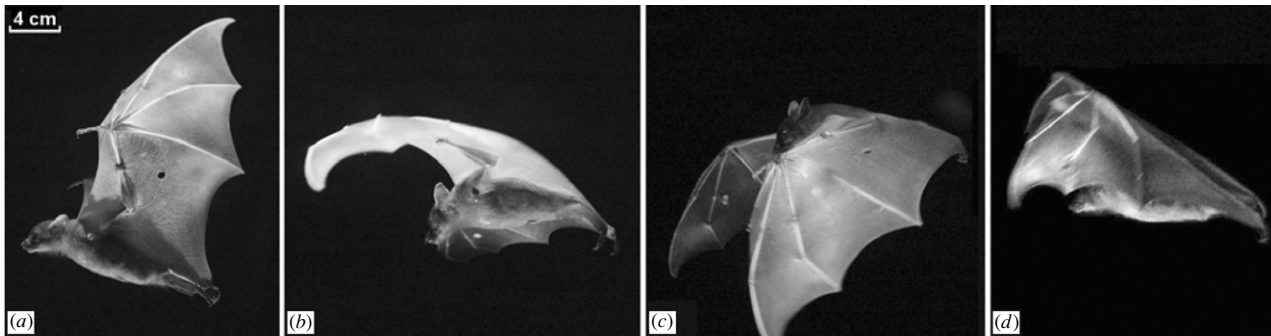


Figure 1. A dog-faced fruit bat (*Cynopterus brachyotis*) in flight. (a) Beginning of downstroke, head forward, tail backward, the whole body is stretched and lined up in a straight line. (b) Middle of downstroke, the wing is highly cambered. (c) End of downstroke, the wing is still cambered. A large part of the wing is in front of the head. (d) Middle of upstroke, the wing is folded toward the body.

and Dickinson 2001, 2002, Ramamurti and Sandberg 2002). Detailed fluid dynamics approaches are now being applied to the study of bird flight as well, including the use of PIV to quantify the velocity fields in wake flows generated by hovering and forward flight (Spedding *et al* 2003a, 2003b; Warrick *et al* 2005). These studies on birds demonstrate that it is possible to analyze the structure of the flow in the wakes of flying vertebrates, and to calculate mechanical and energetic quantities directly from the wake ‘footprint’.

Although biologists and engineers have begun to scratch the surface of insect and bird aeromechanics, studies of flight in bats have yet to make comparable progress. Most investigations of vertebrate flight have assumed that animal aerodynamics can be meaningfully approximated by assuming that bat and bird wings function in the same way as rigid, fixed wings of large, fast, human-engineered aircraft. On this basis, a large biological literature infers maneuverability, flight energetic and other aspects of flight performance and ecology from simple metrics such as aspect ratio and wing loading, particularly for bats (Norberg 1987, Kalcounis and Brigham 1995, McLean and Speakman 2000, Stockwell 2001, Rhodes 2002, Elangovan *et al* 2004). This approach is a reasonable place to start a quantitative analysis of animal flight, but cannot capture all of the relevant functional complexity. In contrast to most fixed-wing aerodynamics, bats fly at a low Reynolds number (10^4 – 10^5), have highly compliant aerodynamic surfaces and are characterized by highly unsteady and three-dimensional wing motions (figure 1), enabled by multiply jointed wing skeletons, thin elastic wing membranes and other specialized morphological features. Understanding the full complexity of bat flight and the ways in which bat flight differs from that of other animals requires attention to the complex functional mechanics and architecture of wings, physiological energetic of locomotion and the kinematics and maneuverability of flight.

As a step toward achieving this goal, we present initial experimental data concerning the kinematics of bat flight and the structure of the wake produced by the characteristic motion of the wings. In the long term, we will be able to apply this information toward clearly defining the unique aerodynamic capabilities of bats and understanding the relationships among bat flight performance and the distinctive morphological and physiological features of this group.

2. Experimental setup

All experiments were performed in an enclosed flight cage located at the Concord Field Station of Harvard University. The flight cage is 8 m long with a cross-sectional area of approximately 1 m (width) \times 2 m (height). As shown in figure 2, the x -axis is defined as the bat’s flight direction, the y -axis is the transverse direction toward to the bat’s left and the z -axis is the vertical direction. The origin of the coordinate system is defined as the point where the bat’s sternum (approximately its center of mass) passes through the PIV laser sheet (discussed below).

Lesser short-nosed fruit bats, *Cynopterus brachyotis*, were the subjects of all tests. We chose this species for analysis because they thrive in captivity, respond well to handling and training and, at a 35–45 g body mass and 30 to 40 cm wing span, are a good size for kinematic and PIV studies. Native to many forested areas of Southeast Asia, a colony of captive-bred individuals have been loaned to us by the Lube Bat Conservancy (Gainesville, Florida). All bats are female, eliminating sex-specific variation. Reflective markers are attached to key anatomical landmarks using medical adhesive. In the flight cage, the average forward speed of bats ranges from 2 to 3 m s^{-1} , at the lower end of their natural range of flight speeds. A top view and a side view of the experimental setup are illustrated in figure 2. The bat flies through the flight cage (from left to right). Her body and wing movements are captured by a pair of Redlake high-speed, low-light sensitive video cameras (MotionScope PCI 1000, operating at a frame rate of 500 images s^{-1}). Both cameras are positioned on the floor looking upwards, with advancing and receding angles. The twin camera arrangement allows for the acquisition of the complete three-dimensional motion of the bat. Low light conditions were preferred because the bats are nocturnal and PIV measurements require a reduced light condition. As the bat flies through the flight cage, it trips a laser beam-break sensor which initiates the data acquisition sequence. After a pre-set delay, typically 300 ms, calculated to allow the bat to pass through the measurement volume, the wake flow is illuminated by a sequence of laser pulses using a pair of Nd:YAG lasers (5 ns, 150 mJ/pulse, typically 1000 μs between adjacent images, 200 ms between adjacent

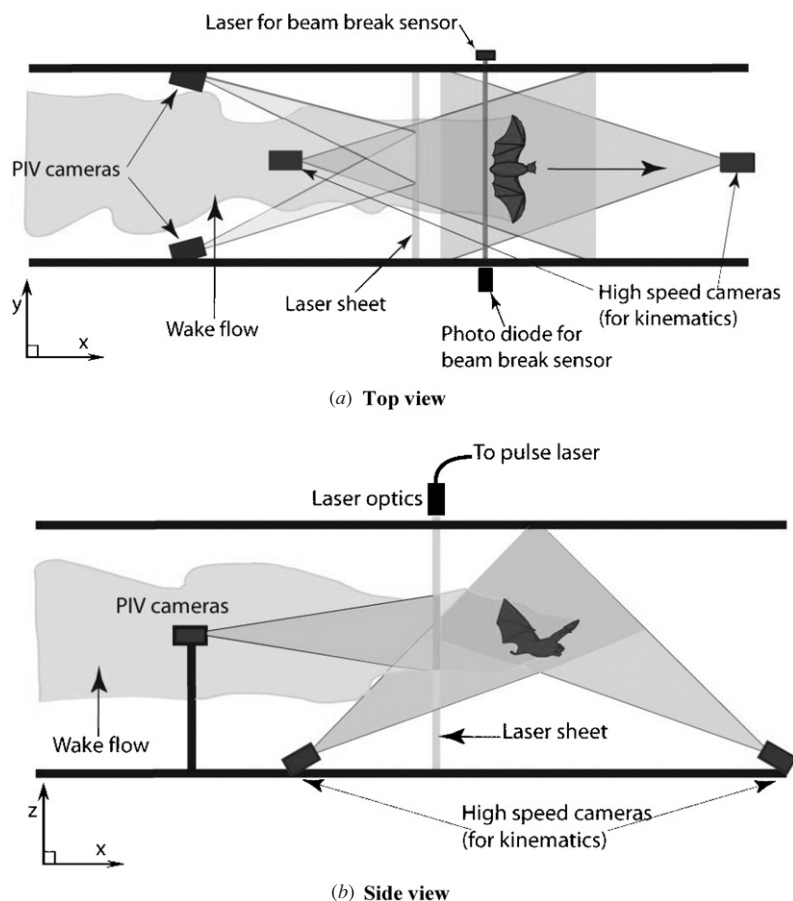


Figure 2. Schematic of the experimental setup for the measurement in the transverse (Treffz) plane. The bat flies from left to right and triggers the acquisition sequence by triggering a beam-break sensor. The wake is imaged in a plane behind the animal, after she has passed through.

image pairs). The laser beam is guided through a series of beam-forming optics which spread out in a thin laser sheet from the flight cage ceiling. The test section is seeded with a light mist of micron-sized aerosol particles of DEHS (di-ethyl-hexyl-sebacate) generated by a custom-built Laskin nozzle fog generator. This fine mist is non-toxic and appears to have no effect on bat behavior. The motion of the tracer particles is captured by a pair of high-resolution CCD cameras (LaVision FlowMaster3 system, image size: 1376×1040 pixels). Both PIV cameras are mounted on a frame and their heights are adjusted at the level of the bat's flight. The velocity field is extracted using standard 3D stereo PIV procedures from the pair of images (LaVision PIV software). By piecing together several image pairs captured from the wake as a function of time, a complete portrait of the wake flow behind the animal can be acquired.

3. Results and discussions

3.1. Straight flight kinematics

Figure 3 shows eight images taken from one of the high-speed camera sequences, recording one whole wing beat. From the video record, one can clearly see the highly articulated motion

of the bat, in contrast to the relatively simple flapping motion of the birds and insects. More than two dozen independently controlled joints in the wing (Vaughan 1970, Swartz 1997) and highly deforming bones (Swartz *et al* 1992, 2005) enable the bat to fly at either positive or negative angle of attack, dynamically change wing camber and create complex 3D wing topology to achieve extraordinary flight performance. Post-processing of the high-speed videos using the direct linear transform (DLT) method merges the separate 2D camera views into a single 3D coordinate space and yields the unsteady three-dimensional motion of the entire wing-body system (Hatze 1988, Tobalske *et al* 2003). A DLT root-mean-square (RMS) error was calculated for each point at every frame. The RMS error varied from frame to frame. The median error was 0.5 cm, 1.25% of the measurement range. Figure 4 shows one such example, the motion of the wing tip relative to the sternum. The open circles are those measured from the stereo video record, and the closed circles indicate points that have been interpolated due to obstruction of the marker point. For each such gap, ten points were selected on either side of the interval. A fifth-order polynomial was then used to fit the data and the gap was filled using this polynomial. The top view indicates that the wing tip outlines a circle during the downstroke, as in birds and insects. During the upstroke, however, the wing

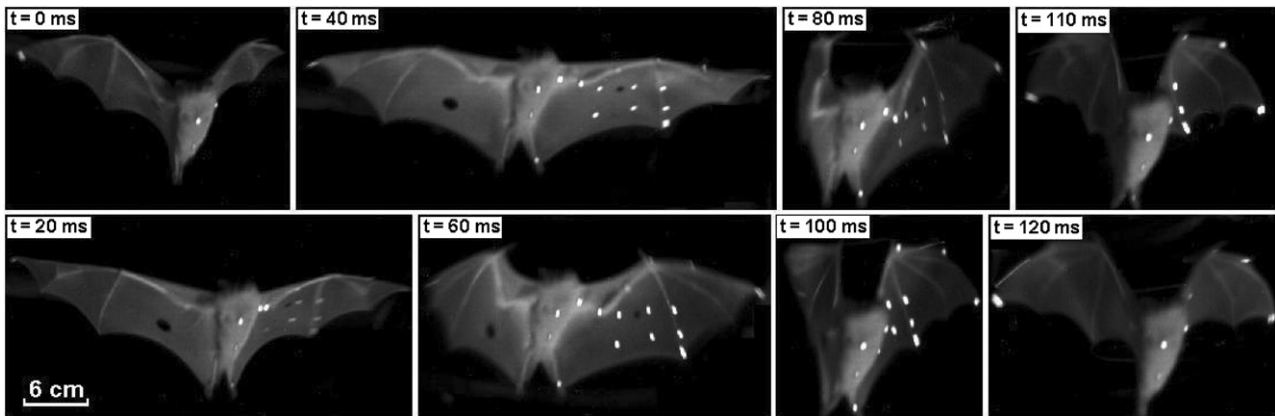


Figure 3. Sequences of images from one high-speed video camera mounted on the test section floor. This view is from below and in front of the bat, which is flying toward the reader. The shoulder, sternum, hip bone and one wing have been marked with reflective markers. These markers are clearly seen when the wing is fully open. During the downstroke, the wing is largely extended, although the joints do not reach full extension. During the upstroke, the substantial flexion of elbow, wrist and finger joints is evident.

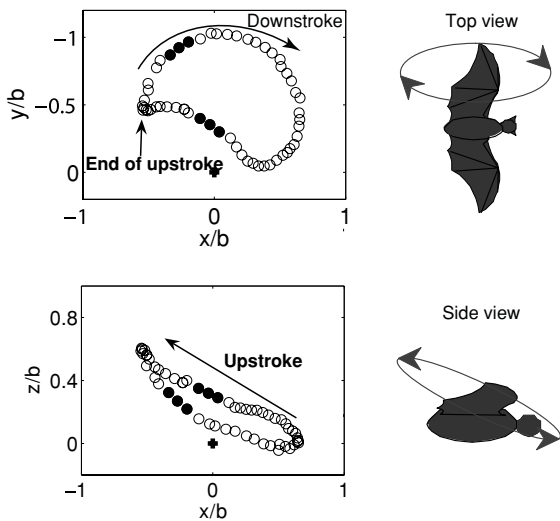


Figure 4. An example of wing tip motion. Shown are a top view (streamwise versus transverse position) and side view (streamwise versus vertical position) of the left wing tip position relative to the sternum marker for a single wing beat (open circles = directly measured position of the wing tip; closed circles = interpolated data; cross = location of the center of the proximal sternum, near the animal's center of mass), and a diagrammatic depiction of the wing tip motion represented by the plots (arrows). The diagrams of the bat represent the related position and direction of movement of the wing tip shown in the plots. b is the half wing span.

tip path is a complex curve. The wing tip is first brought very close to the body. It is then extended away from the body, and at the end of the upstroke it is slightly moved toward the body again. The side view shows that the wing tip moves diagonally from behind the sternum toward the head, and from above to below the sternum during downstroke. The wing tip position is above the sternum for the majority of the wing beat. Both views show that the wing tip position changes more abruptly as the bat begins the downstroke and starts to extend the wing away from the body.

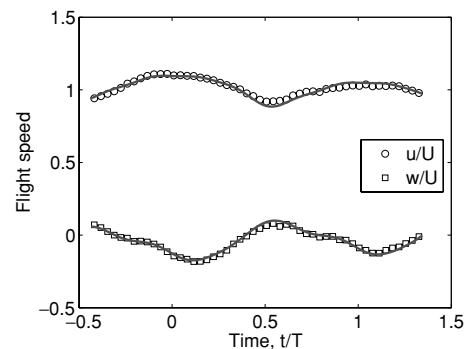
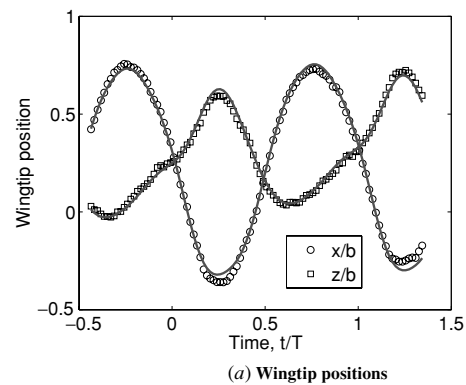


Figure 5. Typical kinematics from bat flight measurements: (a) shows vertical and forward wing tip positions relative to the center of mass while (b) shows the bat flight vertical and forward speeds. The circles and squares are the original data. The solid lines are fitting lines based on (1). U is the bat's forward speed.

The time course of typical wing tip movement relative to the center of mass is shown in figure 5(a). Figure 5(b) shows the forward and vertical flight speeds at the sternum marker, normalized to mean forward speed. The original data obtained from videos are 3D sternum positions varying with time. The flight speeds are calculated by taking the derivative

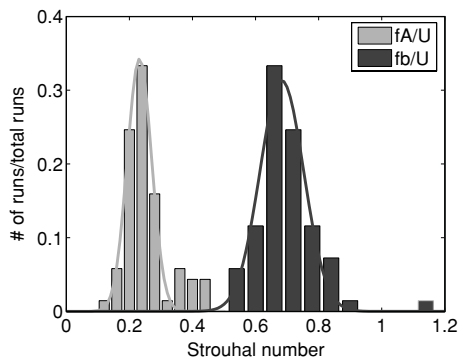


Figure 6. Strouhal numbers. Strouhal numbers were calculated from the kinematic data based on the vertical wing tip amplitude and half wing span, respectively. fA/U is centered around 0.25 which falls within the range of $0.2 < St < 0.4$ given by Taylor *et al* (2003) for cruising flight. fb/U is centered around 0.7, which means in every wing beat the bat flies a distance of $b/0.7$.

of the sternum position. The derivative is calculated from a quadratic polynomial fit to a template of 13 points (six on either side of the point of interest).

The wing beat frequency and amplitude were derived from fitting a Fourier sine series to the wing tip positions:

$$F(t) = C + Bt + \sum_{i=1}^N A_i \sin(i\omega t + \phi_i), \quad (1)$$

where F is the overall wing tip position, C and B are two constants representing the linear trend (for example, if the animal is ascending or descending overall during the flight), t is time, N is the number of Fourier modes, A_i is the amplitude of each mode, ω is the wing flapping frequency $f = \frac{\omega}{2\pi}$ and ϕ_i is the phase offset of each mode. Note that a single frequency is used for all the Fourier modes although each mode is allowed a unique amplitude and phase. The optimal number of Fourier modes, N , was determined by fitting errors. The error was defined as the root-mean-square deviation between the experimental data and the analytical fit. Typically, this error decreased from approximately 5% of the peak-to-peak amplitude ($N = 1$) to less than 1% ($N > 4$). $N = 4$ was used for all fitting presented here.

Using this technique, wing beat frequencies ranged between 7.8 Hz and 10.2 Hz over a total of 67 runs, with an average of 8.81 ± 0.45 Hz (standard deviation). The Strouhal number is often used to describe the wing kinematics of flying animals (Taylor *et al* 2003):

$$St = \frac{fA}{U} \quad \text{or} \quad St = \frac{fb}{U}, \quad (2)$$

where St is the Strouhal number, A is the amplitude of the wing tip vertical movement which is half of the distance between the lowest and highest wing tip positions, b is the half wing span and U is the mean forward speed. The Strouhal number based on wing amplitude, fA/U , ranges from 0.14 to 0.44 with a mean value of 0.25 ± 0.07 (figure 6). The Strouhal number based on half-span, fb/U , ranges from 0.54 to 1.17 with a mean value of 0.7 ± 0.09 (figure 6). All bats used in the tests were trained to fly straight from one end of the

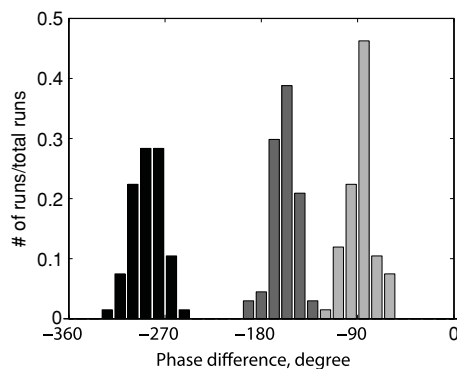


Figure 7. Phase relationships. Wing tip vertical movement (medium dark), vertical flight speed (darkest) and forward flight speed (lightest), all relative to the wing tip horizontal movement. The phase shift in wing tip vertical movement is about $-159 \pm 12^\circ$. It is $-87 \pm 12^\circ$ and $-287 \pm 14^\circ$ in the forward speed and vertical speed, respectively.

flight cage to the other end. During experiments, however, the bat sometimes flew slightly toward the ceiling, or turned to land on a side wall. Both the wing flapping motions and flight speeds change when the bat initiates a turn or stops. The wing tip movements and wing beat frequency also vary among individual bats. The effects of these variations are beyond the scope of the current paper.

Figure 5 illustrates that while the bat flight speed is not constant, it is clearly synchronized with the wing motion. The wing motion in the horizontal plane is largely sinusoidal. However the tip motion in the vertical plane (z) illustrates a higher harmonic of some strength, contributing to the ‘kink’ in the motion during the upstroke, when the animal flexes its wings. The lift or thrust generated by the wing flapping must possess similar periodic variations. From simple rigid body mechanics, a sinusoidal force will exhibit motion whose velocity is 90° out of phase with the force. Histograms of phase differences of the center of mass velocities and wing tip vertical displacement, referenced to the horizontal wing tip motion, clearly show this phase difference (figure 7, lightest). Vertical tip movement is 180° out of phase with the horizontal movement, as would be expected from the patterns in figure 5 (figure 7, medium dark). In addition the vertical flight speed appears to lag the horizontal wing movement by 270° , or more intuitively, to lag the vertical wing displacement by 90° (figure 7, darkest).

3.2. Turning kinematics

We have also acquired some preliminary kinematics for 180° turns. Bats are extraordinarily agile, and these measurements represent some of the first detailed measurements of bats during these extreme maneuvers. Figure 8 shows the trajectory of the bat’s center of mass during a 180° turn. The raw marker positions are shown in the three coordinate axes. As before, closed circles indicate the points that have been interpolated due to marker obstruction. From a purely aerodynamic perspective, the performance of this turn is very impressive. The bat executes a 180° turn in a narrow space of less than a

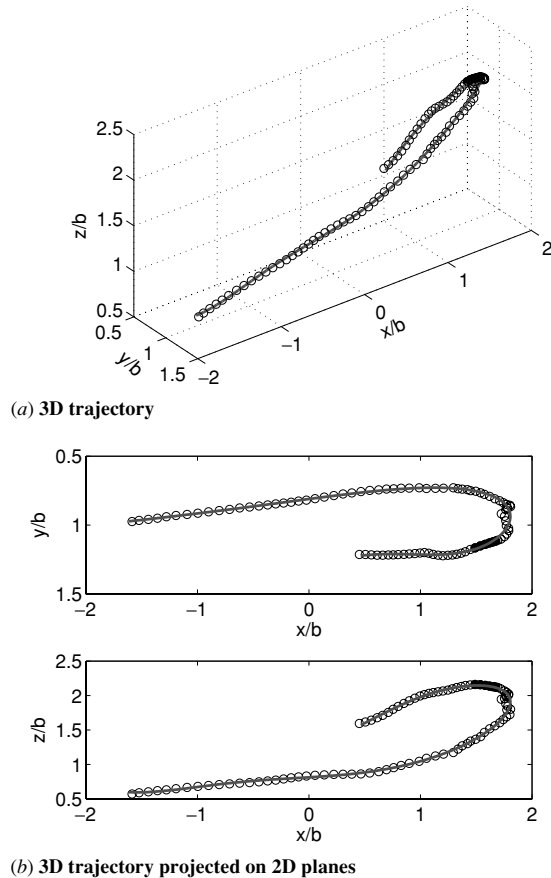


Figure 8. Turning kinematics: (a) shows the location of the sternum during a 180° turn. The bat flies in from the left, rises, turns and flies back again. Views from the top and the side are shown in (b), in the upper and lower frames respectively. Open circles indicate every fifth data point; closed circles are interpolated points where the sternum marker was obstructed from one or both of the camera views.

half of its wing span, and completes the turn within three wing beats ($T = 2-5$). To do this, she flies upwards, turns and drops back down as she flies out in the opposite direction, regaining her incoming velocity almost immediately. Figure 9 shows the bat heading and heading rate during the 180° turn. After the second wing beat ($t/T \sim 2$), the heading slowly changes and the bat prepares for a turn. After the middle of the third wing beat ($t/T = 3.5$), the heading increases in a faster rate, and by the end of the fifth wing beat, the bat has finished the turn ($t/T = 5$). The greater part of the turn is accomplished in less than two wing beats.

3.3. PIV data analysis

PIV images were taken at both the transverse (*Treffz*) and streamwise (*Parasagittal*) planes. Because of the limitations of the PIV system (low sampling rate, limited image view) and the complexity of the bat's flight, PIV data in the streamwise plane will be further investigated at some later time. Discussions here will only focus on the transverse plane where the large-scale vortex structures were most clearly visible. Figure 10

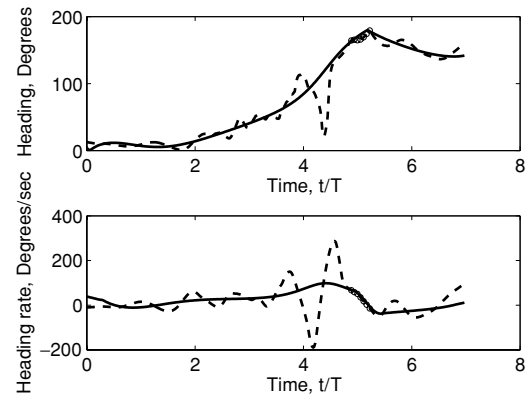


Figure 9. Heading and heading rate during 180° turn. Heading is the angle between the bat flight direction projected on the horizontal plane and the forward x -direction. Heading rate is the change of the heading, calculated from the heading data. The dashed and solid lines represent the instantaneous and average measures respectively. The open circle segment is computed from interpolated data points.

shows a series of wake velocity fields from the transverse plane, behind the left half of the bat, with the coordinate origin centered on the position of the sternum as it pierced the PIV imaging plane. The view of PIV images were $26.5 \text{ cm} \times 20 \text{ cm}$ with a total of 82×62 vectors extracted. Figure 10 shows only one of every four vectors in both rows and columns (a total of 20×15 vectors). It is evident that there is a strong wing tip vortex generated by the bat's flight. The vortex decays in strength, and advects downwards. Since the vortex is well defined, the vorticity, ω , can be determined based on Stokes' theorem from calculation of the circulation, Γ , via contour integration normalized by the area enclosed by the contour composed of differential elements $d\mathbf{r}$ (Batchelor 1967):

$$\iint_A \omega \cdot d\mathbf{A} = \oint \mathbf{u} \cdot d\mathbf{r}. \quad (3)$$

The integration is performed along the edges of 1×1 square interrogation windows using the velocity values at the square's vertices. This vorticity calculation is performed with no oversampling of the interrogation windows and generally provides a more accurate estimate of vorticity than is achieved by differentiation of the velocity field (Raffel *et al* 1998).

The majority of the flow fields measured in this series of experiments exhibit a complexity which makes the task of defining the vortex core difficult. Within the main core itself, there exist smaller vortical structures. Therefore, one cannot simply define the vortex cores as connected regions of vorticity of the same sign. Thus, an alternative method of defining the vortex core was devised to accommodate these nuanced structures so that the circulation could be estimated from these data.

The circulation was only calculated for trials similar to that shown in figure 10, where it was visually apparent that a vortex was located in the measurement plane. According to (3), the circulation of a region can be calculated by integration of the velocity along the contour that is the boundary of this region. For simplicity, this analysis employed circular contours in the circulation calculations. To find the 'center' of the vortex

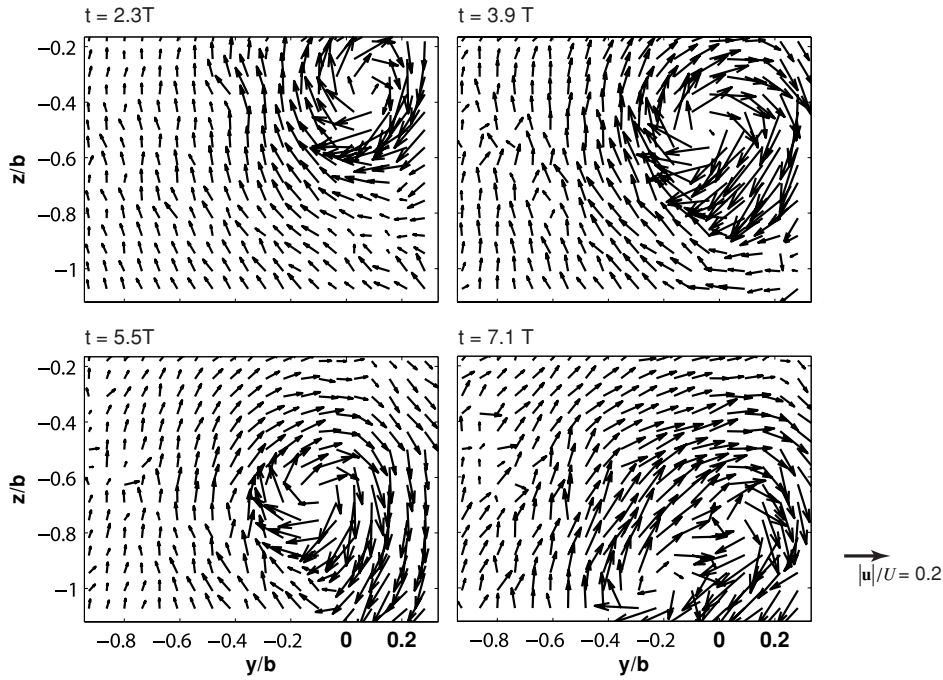


Figure 10. Typical wake velocity fields from PIV images. The origin ($y/b = 0, z/b = 0$) is the point where the center of mass pierced the PIV plane. For this case, the bat passed above the PIV plane. There is a 200 ms separation between successive PIV images. (U : bat’s forward speed; \mathbf{u} : velocity of the wake in a 2D plane. The online version also shows vorticity with color).

core, a rectangular region was manually selected via visual inspection, with care taken to enclose the majority of the main flow structure. The centroid of vorticity within this rectangular interrogation window was then calculated and was defined as the ‘center’ of the vortex core. This location served as the point about which a series of integrations about concentric circular contours of increasing radii were performed to determine the magnitude of the circulation as a function of area enclosed. Utilizing the condition that the flow outside the vortex core is irrotational, the vortex core was defined to be the region within which the circulation reaches a maximum (figure 11). Although the flight is clearly unsteady, we can use the Kutta–Joukowski theorem for steady flight as a crude estimate of the lift per unit span (Anderson 1984):

$$L = \rho U \Gamma, \tag{4}$$

where L is lift per unit span and ρ is air density. Based on the maximum circulation calculated here ($\Gamma/U b = 0.24$, $b = 0.2$ m, $U = 2.7$ m s⁻¹, $\rho = 1.2$ kg m⁻³), the total lift can be approximately estimated as 0.17 N, which, at the measured flight speed, should be able to support a mass of 17 g. This is comparable to, but underestimates, the measured mass (~40 g), but is, at least, in the right neighborhood, considering the simplicity of this argument and the fact that unsteady effects have not been considered. Clearly, more detailed measures of the circulation and its relationship to the true momentum balance need to be performed, although this is not possible with the slow rate of velocity field acquisition (5 Hz, or approximately every two wing beats) that was available to us for this initial set of experiments.

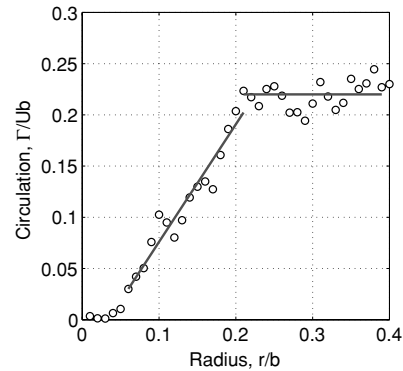


Figure 11. Circulation inside tip vortex. The circulation rises through the vortex core before reaching an approximately constant value of 0.22.

Each PIV acquisition sequence is, however, accompanied by the complete kinematic history of the flight. This enables features identified in the wake structure to be associated with specific wing/body motions. It is, however, a challenge to couple the PIV and 3D kinematic data because runs differ in flight speed and trajectory. To achieve meaningful data synthesis, we first adjust the coordinate origin and normalize velocity. The velocity field is then non-dimensionalized by the flight speed associated with each particular acquisition. Each run is then rearranged and collated based on the wing beat phase angle. In this manner, we are able to determine the location of the vortex core relative to the bat as well as the relative wing location with respect to the wing beat cycle as it moves through the PIV plane. Accordingly, we can reconstruct

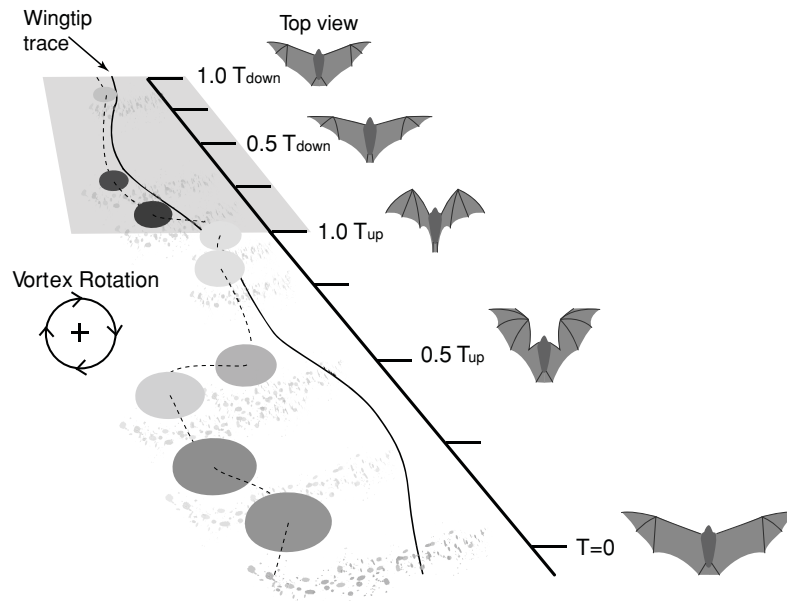


Figure 12. Schematic reconstruction of wake geometry. Wake images are at constant distance downstream of the bat. The darker the vortex color, the stronger is the vorticity.

a ‘cartoon’ of the wake shed by the bat as it moves through its wing beat. Our first attempt at this reconstruction is shown in figure 12, although it should be emphasized that this is hindered by the rather small set of realizations available in the ensemble. The main wing tip vortex structures deposited by the bat on the downstroke closely follow the wing tip trace as one might expect. But, in the case of the upstroke, the vortices shed appear to fall outside the wing tip trace. On the upstroke, the animal folds its wings in toward the body to the point where the wing tips may no longer be the outermost extension of the bat. Therefore, the wake pattern suggests that these upstroke vortices are most likely shed from another location along the folded wing, possibly the wrist joint. With this relatively small and preliminary data set, it is too early to be able to say how this cartoon compares with wake vortex structures proposed for the case of bird flight (Rayner 1979, 1987, Spedding *et al* 2003), and more detailed studies are clearly required.

4. Conclusions

We have performed experiments to capture the coupled kinematics and wake velocities of bats. The kinematics reveals that, at the relatively low flight speeds considered here, bats possess unique flight characteristics, distinct from those observed in both insect and bird flight, including a flexion of the wing during the upstroke compared to the largely extended sweep that characterizes the middle portion of the downstroke. We have also characterized maneuvering flight, in particular a 180° turn, which the bat executes rapidly over a short distance and narrow radius, exhibiting turn rates exceeding 200° s^{-1} . The kinematic data also show that the flight speed and elevation are not constant, but are closely synchronized with wing horizontal and vertical motions. We have successfully employed PIV data to reconstruct wake geometry which

indicates strong wing tip vortices and a complex vortical wake structure, although these need to be verified and explored further. The experiments presented in this paper represent the first detailed measurements to couple wing kinematics and wake velocities of bats, and further research will increase both data quantity and quality. As available instrumentation improves, new experiments will yield more insights into the abilities and underlying biomechanics that these animals exhibit.

Acknowledgments

All experiments were conducted at the Concord Field Station (CFS) at Harvard University and we express our thanks to the CFS staff, especially Andy Biewener, the director of CFS, for his support. We gratefully acknowledge the support of the Lubee Bat Conservancy, especially Dr Allyson Walsh and Dana LeBlanc. We are also most grateful to Dr Ty Hedrick for his assistance, and for the use of his kinematics digitizing code. The work is supported by the Air Force Office of Scientific Research (AFOSR), monitored by Dr R Jeffries and W Larkin, NSF, and the Brown University UTRA program.

References

- Alexander R M 2003 *Principles of Animal Locomotion* (Princeton, NJ: Princeton University Press)
- Anderson J 1984 *Fundamentals of Aerodynamics* (New York: McGraw-Hill)
- Batchelor G 1967 *An Introduction to Fluid Dynamics* (Cambridge: Cambridge University Press)
- Biewener A A 2003 *Animal Locomotion* (Oxford: Oxford University Press)
- Birch J M and Dickinson M H 2001 Spanwise flow and the attachment of the leading-edge vortex on insect wings *Nature* **412** 729–33

- Blickhan R and Full R J 1993 Similarity in multilegged locomotion—bouncing like a monopode *J. Comp. Physiol. A* **173** 509–17
- Cavagna G A *et al* 1977 Walking, running and galloping: mechanical similarities between different animals *Scale Effects in Animal Locomotion* ed T J Pedley (New York: Academic) pp 111–26
- Dickinson M 2001 Solving the mystery of insect flight—insects use a combination of aerodynamic effects to remain aloft *Sci. Am.* **284** 48–57
- Dickinson M H *et al* 2000 How animals move: an integrative view *Science* **288** 100–6
- Edwards R H and Cheng H K 1982 The separation vortex in the Weis-Fogh circulation-generation mechanism *J. Fluid Mech.* **120** 463–73
- Elangovan V *et al* 2004 Wing morphology and flight performance in *Rousettus leschenaulti* *J. Mammal.* **85** 806–12
- Ellington C P 1984 The aerodynamics of hovering insect flight. Parts I–VI *Phil. Trans. R. Soc. Lond. B* **305** 1–181
- Farley C T and Ferris D P 1998 Biomechanics of walking and running: from center of mass movement to muscle action *Exercise Sport Sci. Rev.* **26** 253–85
- Farley C T and McMahon T A 1992 Energetics of walking and running—insights from simulated reduced-gravity experiments *J. Appl. Physiol.* **73** 2709–12
- Grodnitsky D L and Dudley R 1996 Vortex visualization during free flight of heliconiine butterflies (Lepidoptera: Nymphalidae) *J. Kansas Entomol. Soc.* **69** 199–203
- Hatze H 1988 High-precision three-dimensional photogrammetric calibration and object space reconstruction using a modified DLT-approach *J. Biomech.* **21** 533–8
- Heinzel H-G and Gewecke M 1987 Aerodynamic and mechanical properties of the antennae as air-current sense organs in *Locusta migratoria*: II. Dynamic characteristics *J. Comp. Physiol. A* **161** 671–80
- Kalcounis M C and Brigham R M 1995 Intraspecific variation in wing loading affects habitat use by Little Brown bats (*Myotis Lucifugus*) *Can. J. Zool.* **73** 89–95
- Liu H *et al* 1998 A computational fluid dynamic study of hawkmoth hovering *J. Exp. Biol.* **201** 461–77
- McLean J A and Speakman J R 2000 Morphological changes during postnatal growth and reproduction in the brown long-eared bat *Plecotus auritus*: implications for wing loading and predicted flight performance *J. Nat. Hist.* **34** 773–91
- Müller U K *et al* 2000 Hydrodynamics of unsteady fish swimming and the effects of body size: comparing the flow fields of fish larvae and adults *J. Exp. Biol.* **203** 193–206
- Norberg U M 1987 Wing form and flight mode in bats *Recent Advances in the Study of Bats* ed M B Fenton, P Racey and J V M Rayner (Cambridge: Cambridge University Press) pp 43–56
- Raffel M *et al* 1998 *Particle Image Velocimetry: A Practical Guide* (New York: Springer)
- Ramamurti R and Sandberg W C 2002 A three-dimensional computational study of the aerodynamic mechanisms of insect flight *J. Exp. Biol.* **205** 1507–18
- Rayner J M V 1979 A vortex theory of animal flight: II. The forward flight of birds *J. Fluid Mech.* **91** 731–63
- Rayner J M V 1987 The mechanics of flapping flight in bats *Recent Advances in the Study of Bats* ed M B Fenton, P Racey and J V M Rayner (Cambridge: Cambridge University Press) pp 23–42
- Rhodes M P 2002 Assessment of sources of variance and patterns of overlap in microchiropteran wing morphology in southeast Queensland, Australia *Can. J. Zool.* **80** 450–60
- Sane S P and Dickinson M H 2001 The control of flight force by a flapping wing: lift and drag production *J. Exp. Biol.* **204** 2607–26
- Sane S P and Dickinson M H 2002 The aerodynamic effects of wing rotation and a revised quasi-steady model of flapping flight *J. Exp. Biol.* **205** 1087–96
- Spedding G R *et al* 2003a A family of vortex wakes generated by a thrush nightingale in free flight over its entire range of flight speeds *J. Exp. Biol.* **206** 2313–44
- Spedding G R *et al* 2003b Quantitative studies of the wakes of freely flying birds in a low-turbulence wind tunnel *Exp. Fluids* **34** 291–303
- Stockwell E F 2001 Morphology and flight manoeuvrability in New World leaf-nosed bats (Chiroptera: Phyllostomidae) *J. Zool.* **254** 505–14
- Swartz S M 1997 Allometric patterning in the limb skeleton of bats: implications for the mechanics and energetics of powered flight *J. Morph.* **234** 277–94
- Swartz S M *et al* 1992 Wing bone stresses in free flying bats and the evolution of skeletal design for flight *Nature* **359** 726–9
- Swartz S M *et al* 2005 Dynamic complexity of wing form in bats: implications for flight performance *Functional and Evolutionary Ecology of Bats* ed Z Akbar, G McCracken and T H Kunz (Oxford: Oxford University Press)
- Taylor G K *et al* 2003 Flying and swimming animals cruise at a Strouhal number tuned for high power efficiency *Nature* **425** 707–11
- Tobalske B W *et al* 2003 Wing kinematics of avian flight across speeds *J. Avian Biol.* **34** 177–84
- VandenBerg C and Ellington C P 1997a The three-dimensional leading-edge vortex of a ‘hovering’ model hawkmoth *Phil. Trans. R. Soc. Lond. B* **352** 329–40
- VandenBerg C and Ellington C P 1997b The vortex wake of a ‘hovering’ model hawkmoth *Phil. Trans. R. Soc. Lond. B* **352** 317–28
- Vaughan T A 1970 The skeletal system *The Biology of Bats* vol 1 ed W A Wimsatt (New York: Academic) pp 98–139
- Warrick D R *et al* 2005 Aerodynamics of the hovering hummingbird *Nature* **435** 1094–7
- Willmott A P and Ellington C P 1997a The mechanics of flight in the hawkmoth *Manduca sexta*: I. Kinematics of hovering and forward flight *J. Exp. Biol.* **200** 2705–22
- Willmott A P and Ellington C P 1997b The mechanics of flight in the hawkmoth *Manduca sexta*: II. Aerodynamic consequences of kinematic and morphological variation *J. Exp. Biol.* **200** 2723–45